PHYSICAL REVIEW C VOLUME 41, NUMBER 4 APRIL 1990

Measurement of the beta spectral shapes of ^{12}B and ^{12}N

Jordan B. Camp*
University of Chicago, Chicago, Illinois 60637

(Received 25 September 1989)

The spectral shapes of the ^{12}B and ^{12}N beta decays have been measured with a beta spectrograph specifically designed to examine the spectral effect of weak magnetism. Writing the weak magnetism correction to the beta spectra as $(1+\alpha_{\pm}E)$ we find the difference $\alpha_{-}-\alpha_{+}=(1.24\pm0.42)\%/\mathrm{MeV}$, in agreement with the conserved vector current prediction.

INTRODUCTION

The conserved vector current (CVC) theory relates the electromagnetic and weak vector hadronic currents.[1] According to CVC the charge changing weak currents and the isovector electromagnetic current may be identified as the three isospin components of a single conserved isovector current. There follows a simple relationship between the form factors associated with these currents.

CVC may be tested through the comparison of form factors extracted from analog weak and electromagnetic decays. The weak form factors may be obtained from the observables of nuclear beta decay, the beta angular distribution from aligned nuclei and beta spectral shapes. Alignment studies have verified CVC to the 10% level.[2] The status of CVC with regard to spectral shapes has been less clear.

In particular the $A=12$ system provides a suitable means for testing CVC.[3] The shape of the beta decay spectra are used to determine the weak magnetism form factor $F_m(0)$, while the analog electromagnetic form factor is extracted from knowledge of the radiative width of the analogous electromagnetic decay (obtained by inelastic electron scattering). Early experiments found indications of the relationship predicted by CVC.[4,5] The next generation experiment, initially in agreement with theory, was later met with controversy.[6-8] An additional experiment found a comparison of the beta shapes in agreement with theory at the 10% level, although the individual shapes themselves were not in agreement.[9]

The momentum spectrum for the mass 12 beta decays may be written as follows:

$$dN_{\pm}=\frac{4G^2}{(2\pi)^3}\cos^2\Theta_c[R(E,E_0)F_{\pm}(Z,E)p^2(E-E_0)^2]\times(1+\alpha_{\pm}E)dp\ .$$

The expression in brackets represents an allowed shape with electromagnetic corrections: $+(-)$ refers to positrons (electrons), p and E are the beta momentum and energy, R is the radiative correction, and F is the Fermi function. The $(1+\alpha_{\pm}E)$ term represents a modification to the allowed spectrum of order $F_m(0)E/m_pc^2$, predicted by CVC to be roughly $\mp 0.5\%/\mathrm{MeV}$.[2] It is the purpose of this paper to report a new measurement of the spectral shapes of ^{12}N and ^{12}B. The shape determination has been done with a beta spectrograph designed to minimize systematic errors associated with the measurement of high-energy nuclear beta spectra.

PHILOSOPHY OF DESIGN

The beta spectrograph was designed with the specific goal of measuring the effects of weak magnetism on the beta decay spectrum. The following criteria were factors in the choice of the final design.

(1) *Acceptance of a large momentum bite.* Weak magnetism is an effect that extends across the entire beta spectrum. The smallness of the effect ($\sim$0.5%/MeV) demands the measurement of a relatively large portion of the spectrum. To avoid these errors encountered in combining separate measurements of discrete portions of a beta spectrum, the spectrograph should accept a large momentum bite ($\sim$50%).

(2) *Insensitivity to spectrograph resolution.* The observation of weak magnetism is not critically dependent on resolution, which is more important for the detailed measurement of a small portion of the spectrum.

(3) *Electron scattering.* The effects of electron scattering must be minimized. This includes scattering at the source, entrance aperture and detector.

(4) *Geometrical simplicity.* The outstanding problem in the measurement of high-energy nuclear beta spectra is the lack of monoenergetic electron sources >1 MeV to provide energy calibration. Since less direct methods must be used, electron orbits through the spectrograph should be kept as simple as possible.

The design believed to best satisfy these criteria is shown in Fig. 1. It is a flat-field iron core magnet using active collimation and instrumented with gas proportional counters. An accepted event must pass through the aperture of an active collimator, trigger a thin (2.0 mg/cm^2) counter, traverse the magnet in a semicircular path, and finally pass through a low mass drift chamber and thin scintillator. A 50% momentum bite is accepted. Other advantages of this design are the ability to reconstruct beta trajectories that give information about source position, beta scattering, spectrograph resolution, etc. and the multicoincidence requirement that provides a very low background instrument. The spectrograph

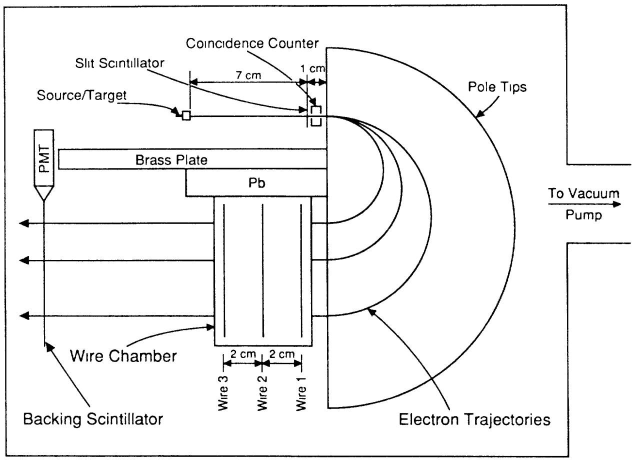

FIG. 1. Side view of spectrograph.

geometry (described in the following) fixes the acceptance at $d\Omega/4\pi \sim 5\times10^{-5}$ and the resolution at beta energies >7 MeV at $\Delta p/p \sim 3\%$.

GENERAL DESCRIPTION OF INSTRUMENT

The spectrograph can be considered as consisting of four sections: the source, the entrance aperture, the magnet system and the detection system.

(1) *Source.* The source was generated by the Los Alamos tandem accelerator beam. A circular beam spot ~ 2 mm in diameter was projected on target through two tantalum collimators spaced 7 cm apart. The target material was evaporated onto a 1 mg/cm^2 Be backing in a 2-mm spot to ensure object stability in spite of beam wandering.

(2) *Entrance Aperture.* A partial condition for an event to be accepted by the spectrograph is that it pass through a thin wire chamber without activating an anticoincidence collimating scintillator. These counters are called the coincidence counter and slit, respectively. The slit is an active collimator that defines the entrance aperture to the spectrograph. It is a 1.9×1.3 cm, 0.08-cm thick NE102 plastic scintillator with a 2-mm diameter hole located 7 cm from the target. The hole allows for beta takeoff angles of $0-(\pm1.6°)$. The use of the slit anticoincidence condition minimizes the effect of slit scattering on the beta spectrum. The coincidence counter is a wire chamber 1-cm thick and uses an 80% Ar, 20% CO$_2$ mixture at 380 Torr. Mylar windows and gas each contribute 1 mg/cm^2 mass. The counter is run at high gain and is used to indicate that a beta has entered the magnet through the entrance aperture. The requirement of a signal from the coincidence counter serves to eliminate background that could otherwise trigger the detection system without actually passing through the entrance aperture. Background rejection is crucial because the momentum calibration involves a careful examination of the endpoint region.

(3) *Magnet.* The magnet is a 180° flat-field dipole magnet with Hall-probe feedback. The pole tips are soft iron, with a semicircular shape of radius 15 cm. The gap is 2.1 cm. A maximum and minimum radius of curvature of 9.7 and 5.1 cm, respectively, allows a momentum bite of $\Delta p/p_{\mathrm{max}}=0.47$.

(4) *Detector.* Upon exiting the magnet an accepted beta ray must pass through both a three-wire drift chamber and a backing plastic scintillator. The drift chamber, operated with 80% Ar 20% Co$_2$ gas at 580 Torr, consists of three parallel wires mounted 0.5 cm behind a ground plane defining the end of a 5-cm drift field region. The wires are 13-cm long, 10-μm diameter Moleculoy with a resistivity of 180 Ω/cm. They are separated by 2 cm and are perpendicular to the drift field. A measurement of drift time of the ionized trail to the wires and position along the wires (obtained from charge division) then provides the trajectory of the beta through the magnet, and hence its momentum. (Trajectories are also used to provide information on spectrograph resolution, beta scattering, etc.)

A measurement of a beta trajectory using any two wires can be used to predict the measurement on the third. The difference between the prediction and an actual measurement will then give the detector resolution. We have found the timing resolution to be 0.02 μsec (corresponding to 0.5 mm) and the position resolution to be 2 mm.

Located 10 cm behind the drift chamber is a single long thin plastic scintillator (5.5-cm wide$\times$10-cm long$\times$0.16-cm thick). The scintillator serves both to reject background by reducing the number of acceptable trajectories through the drift chamber and also provides the fast timing reference for the wires.

A valid event requires an above threshold signal from the coincidence counter, the backing scintillator and at least one wire in the drift chamber, and has no signal from the entrance slit anticoincidence counter.

DATA COLLECTION

The reactions used to generate the beta decay sources were ^{11}B$(d,p)^{12}$B with $E_d=2$ MeV and ^{10}B(^{3}He$,n)^{12}$N with $E_{^3\mathrm{He}}=8$ MeV. The targets were 1 mg/cm^2 ^{11}B and 6 mg/cm^2 ^{10}B deposited on 1 mg/cm^2 Be backing. Cross sections of ~ 500 mb for ^{12}B and ~ 5 mb for ^{12}N gave event rates of 10 and 3 per second, respectively.

The experimental procedure consisted of target irradiation by the Los Alamos tandem Van de Graaff beam for one parent half-life (beam on) followed by data collection for the same length of time (beam off). While the beam was on the coincidence counter and drift chamber were exposed to large radiative fluxes. To prevent these counters from suffering voltage breakdowns and general deterioration it was necessary to lower their bias voltage by $\sim 15\%$ so that they were no longer in proportional mode when the beam was on. The raw data of the ^{12}B and ^{12}N beta spectra are shown in Fig. 2 with an allowed shape normalized to the total number of counts drawn through the data.

Also measured was the 3.35 MeV e^- conversion line from ^{40}Ca* which requires a 15 mg/cm^2 Ca target mounted on a 100 mg/cm^2 carbon backing. The reaction used was ^{40}Ca$(p,p')^{40}$Ca* with $E_p=5.2$ MeV; the thick target backing was needed to shield the spectrograph from scattered protons and secondary particles during this electromagnetic (beam on) measurement.

SPECTROGRAPH MOMENTUM CALIBRATION

The relation between a beta ray of momentum p and its radius of curvature ρ in a uniform magnetic field B is given by

$$p(\mathrm{MeV}/c)=0.2998\times B(\mathrm{kG})\times\rho(\mathrm{cm}) .$$

The quantity ρ is measured by determining the distance between the entrance aperture to the magnet and the detected beta. We have

$$2\rho=R_0+kC ,$$

where R_0 is the distance between the center of the entrance aperture and the low-energy end of the drift chamber wires, C is a channel number obtained from charge division, and k is a constant relating channel number to position along the wire.

Determination of k. Figure 3 shows the 3.35-MeV electron conversion line from the decay of the first excited state of ^{40}Ca measured at the magnetic-field settings of 1.51 and 2.15 kG. (The large background present is due to e^+e^- production from this and the $2-$ and $3+$ states; also, drift chamber multiple scattering at this energy broadens the resolution of this line to ~6%.) The centroid of each peak was measured to an accuracy of ±0.5 channel, giving a value of $k=0.0483\pm0.0003$ cm/channel. The effect of fringe field saturation (discussed later) modifies this value to 0.0481 for ^{12}B and 0.0480 for ^{12}N.

Determination of R_0. Calibration with low-energy electron conversion line sources (e.g., ^{207}Bi) was not possible as the steep onset of multiple scattering in the detectors precludes measurements of betas at energies <3

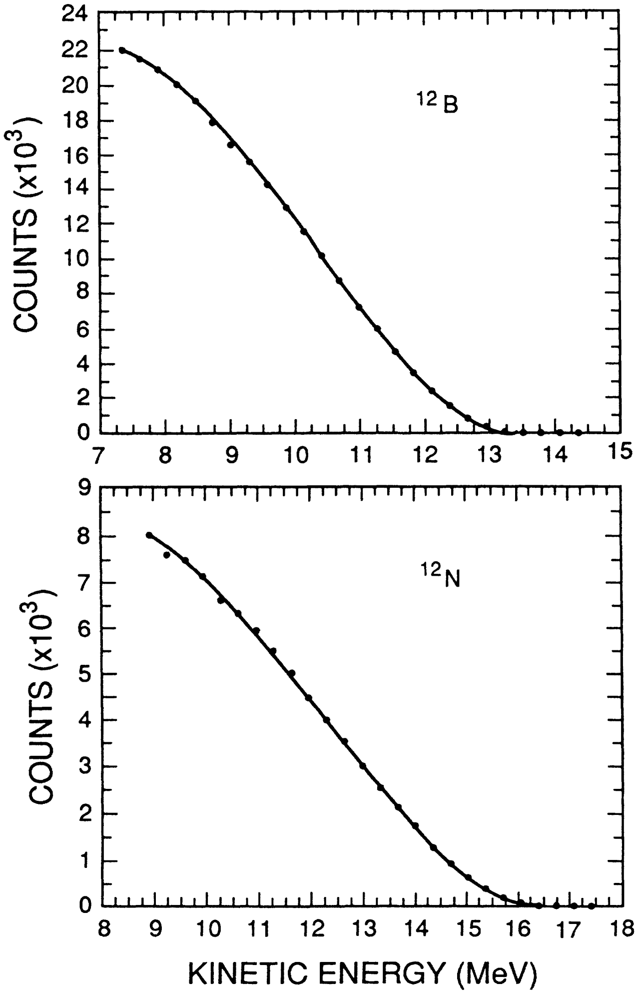

FIG. 2. The observed beta spectra of ^{12}B and ^{12}N. The data, fit with allowed shapes, are shown without corrections.

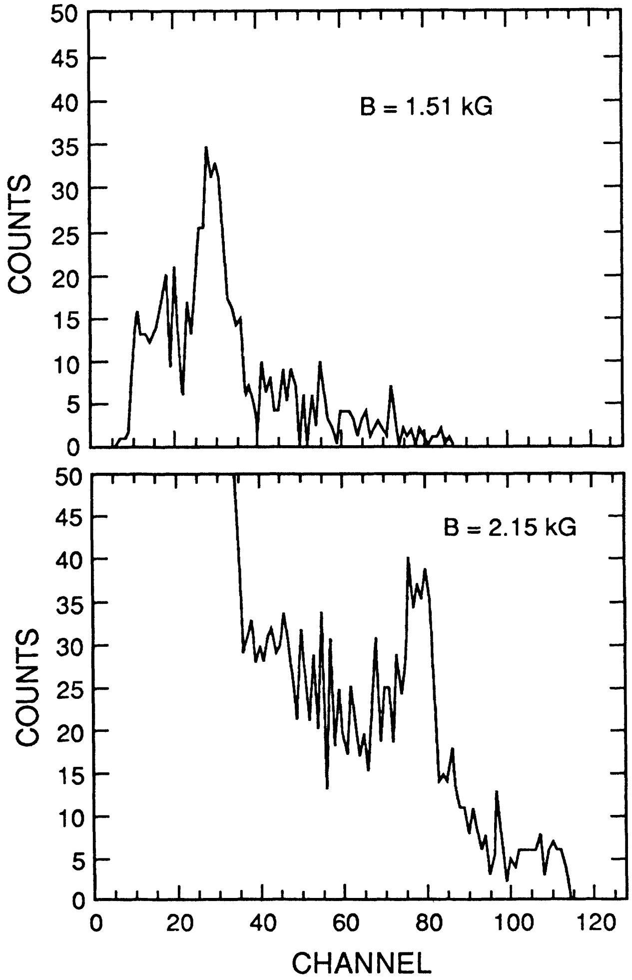

FIG. 3. The 3.35-MeV electron conversion line from ^{40}Ca. Multiple scattering at this energy broadens the resolution to ~6%.

MeV. Instead, the method used to determine R_0 depends on the spectral shape factor, which is defined by the operation of dividing the measured spectrum by a calculated allowed shape. The upper energy 10% of the shape factor (S) will show a strong dependence on a miscalibration of the assigned momentum, rising or falling steeply depending on the sign of the error.

With p=actual momentum, p'=assigned momentum, E=beta energy, E_0=endpoint energy, near the endpoint the behavior of S can be approximated by

$$S=\frac{1+aE}{1+\frac{2(p'-p)}{(E_0-E)}} ,$$

where a is a constant that absorbs the electromagnetic and weak magnetism spectral corrections. For $p'\neq p$ (miscalibration), S diverges near the endpoint. R_0 is then fixed to obtain nondivergent behavior of the shape factor at the endpoint.

In practice, an initial value of R_0 was chosen. After subtracting background (see the following), the branching ratios of 2.1% and 1.3% for ^{12}N and ^{12}B, respectively, were used to remove the spectral effects of branches to the 4.43-MeV state in ^{12}C.[8] The corrected spectrum was then divided by an allowed shape (using the endpoint energies, corrected for nuclear recoil, of 16.833 and 13.370 MeV for ^{12}N and ^{12}B), leaving the shape factor, to which a straight line was fit. The χ^2 was then measured of the last 10% of the fit. The process was repeated for various values of R_0; R_0 was chosen so that χ^2 was minimized.

Figure 4 shows the application of the calibration procedure to the measured ^{12}B spectrum. The shape factor is shown for two values of R_0 differing by only 0.02 cm, with a large change in the total χ^2 for the last three points: $\chi^2(R_0=4.25\ \text{cm})=1.5$, while $\chi^2(R_0=4.27\ \text{cm})=11$.

χ^2 (for the last three points) is then plotted vs R_0 for both ^{12}B and ^{12}N (measured with the same value of R_0) in Fig. 5(a). In Fig. 5(b) the χ^2 for the two spectra is

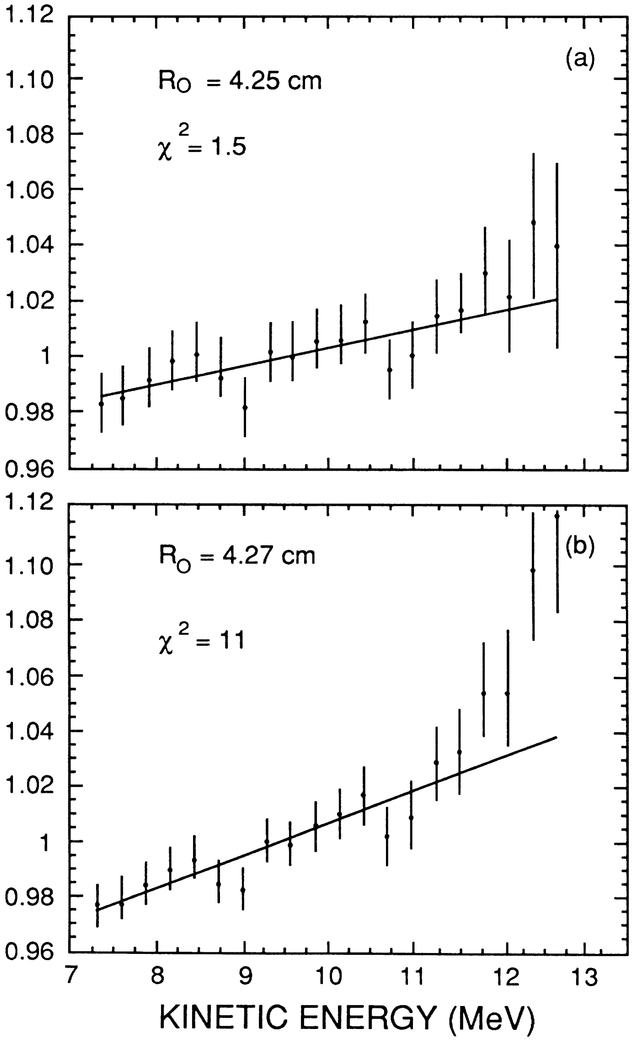

FIG. 4. The ^{12}B shape factor dependence on momentum calibration.

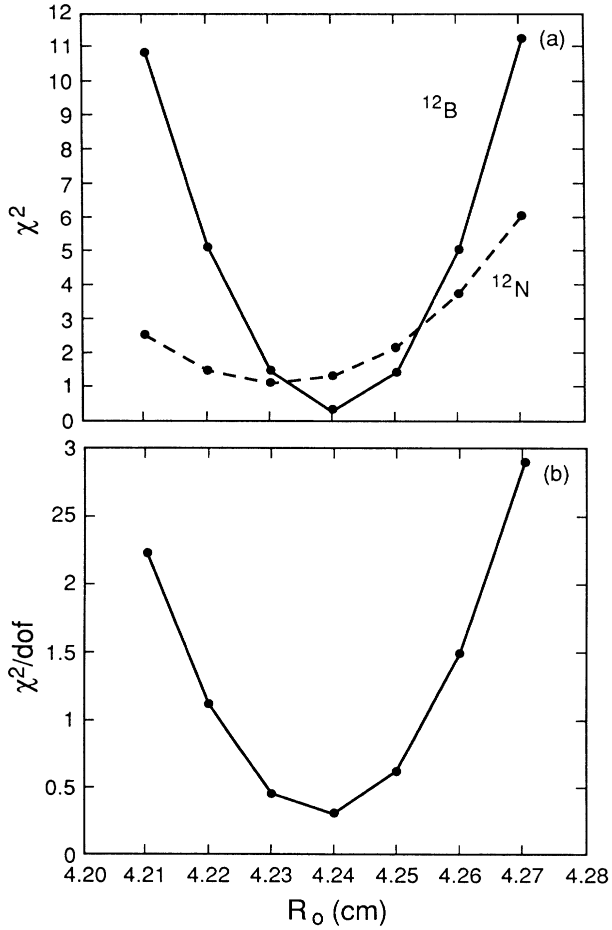

FIG. 5. Spectrograph momentum calibration. (a) The shape factor χ^2 plotted against the constant R_0 for the ^{12}B and ^{12}N spectra. (b) The χ^2 for the two spectra is summed. Acceptable values of R_0 are those with χ^2/dof < 1.2.

summed. Taking acceptable values of R_0 to be those with $\chi^2/\mathrm{dof} \leq 1.2$, we find $R_0 = 4.24 \pm 0.02$ cm.

Having determined the calibration, the slope of the shape factor (in %/MeV) is measured. The preceding uncertainties in k and R_0 correspond to an error of ~0.5%/MeV in individual spectral slope and an error of 0.09%/MeV for the ^{12}B$-^{12}$N difference.

BACKGROUND

The nature of the background has been investigated by using a TAC spectrum between fast timing signals from the scintillator and the coincidence counter, shown in Fig. 6(a). It was found that counts beyond the beta spectrum endpoint energy corresponded to counts uniformly distributed in time in the TAC spectrum; thus a background event in the measured beta spectrum consisted of a beta triggering the drift chamber and scintillator in accidental coincidence with a beta activating the coincidence counter. Background was examined by selecting the events outside of the TAC peak—the background spectrum from ^{12}N is shown in Fig. 6(b). The total background rates for both ^{12}N and ^{12}B were ~0.2% of the total measured beta spectrum counting rate.

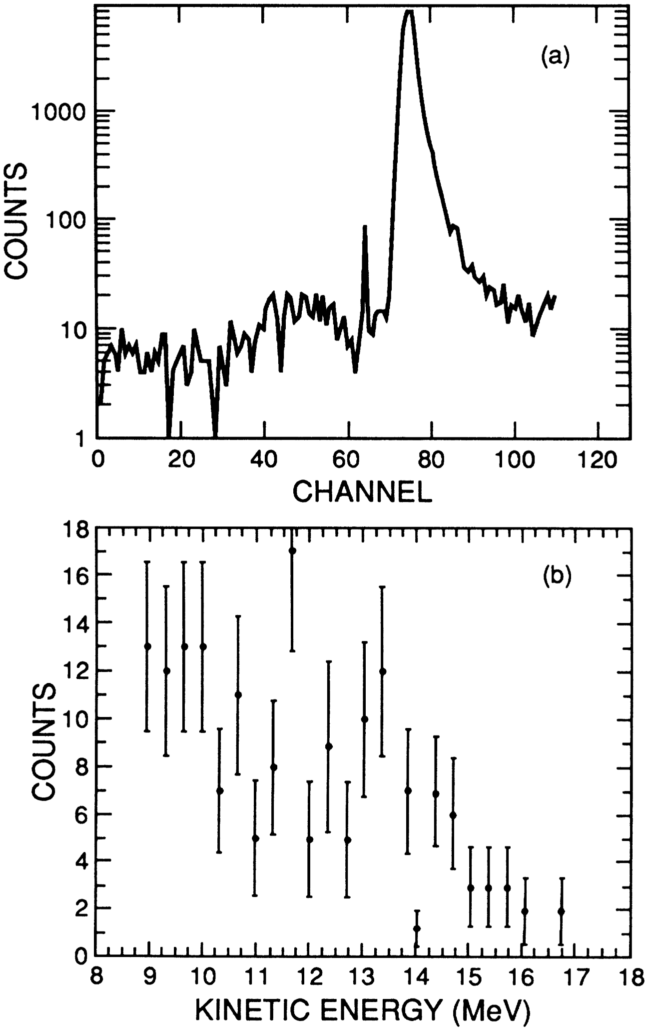

FIG. 6. Determination of background. (a) TAC spectrum between backing scintillator and coincidence counter. (b) ^{12}N background spectrum generated by selecting events outside the TAC peak.

SYSTEMATIC ERRORS

In this section the effect of instrumental systematics on measured beta spectra are discussed.

Source position. The targets, 2 mm in diameter, were illuminated by the accelerator beam in an uncontrolled but approximately uniform fashion. Beam wandering across the target will result in a change in the calibration constant R_0: a 1-mm beam misalignment with respect to the target center gives a 0.5-mm change in R_0. As the spectra from the decays of ^{12}N and ^{12}B were directly compared it was important to establish that beam wandering did not cause a shift of R_0 between the two spectra. This was done by examining the spectrum position alignment (PA), generated by taking the difference between beta position on wire three and wire one for each event; a change in source position Δy will project into a change ~0.5 Δy in PA peak position. It was found that

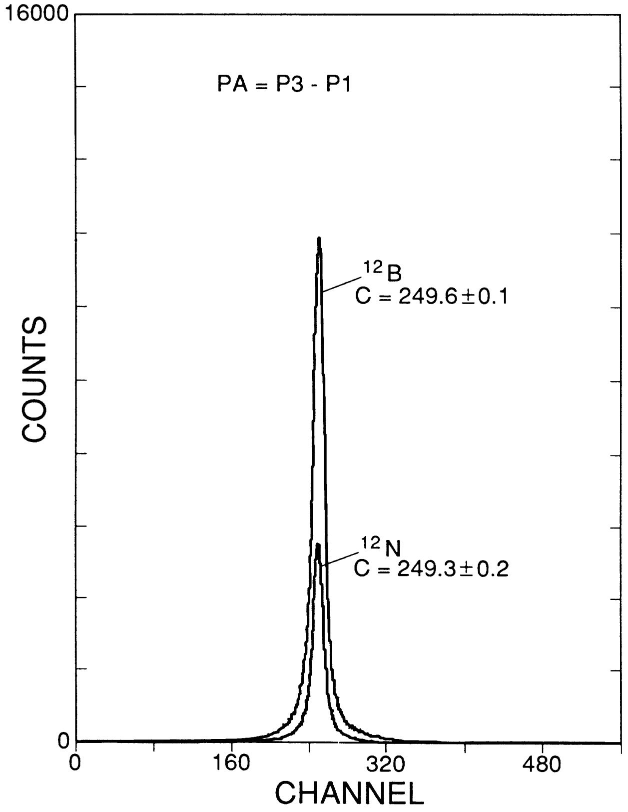

FIG. 7. Spectrum PA, generated by taking the difference $P3-P1$ for each event.

TABLE I. Summary of errors.

Source of error	Effect on spectrum (%/MeV) ^{12}B	^{12}N	^{12}B-^{12}N
Calibration	0.5	0.5	0.09
Systematic errors			
Magnetic-field shape	0.06	0.06	0.01
Source position		0.08	0.08

the centroid of PA shifted by ~0.2% (corresponding to $\Delta R_0=0.004$ cm) between the ^{12}B and ^{12}N runs (Fig. 7). This shift is within the statistical accuracy of the measurement of the centroids. Since the ^{12}B spectrum has comparatively high statistics and essentially provides the calibration, we ascribe an uncertainty of 0.08%/MeV (corresponding to $\Delta R_0=0.004$ cm) to both the ^{12}N spectral shape and the $^{12}\mathrm{B}-{}^{12}\mathrm{N}$ difference.

Magnet. Both resettability (after changing the field direction) and stability over a 24 h period were good to ±0.02% (measured with a Spectromagnetics NMR gaussmeter).

A careful examination of the magnetic field shape was undertaken so that calculations of beta trajectories through the magnet could be done to high precision (0.1% level). The following fields were used in the experiment: 1.5 and 2.14 kG for the ^{40}Ca electron conversion line, 4.8 kG for ^{12}B and 5.8 kG for ^{12}N. The magnetic field was mapped using a Bell 811A Hall probe (0.1% linearity from 0–10 kG) at fields of 1.5, 2.3, 4.8, and 5.8 kG. At the higher field settings of 4.8- and 5.8-kG fringe field saturation (i.e., a nonlinear response of field to magnet current) at the several per cent level was found.

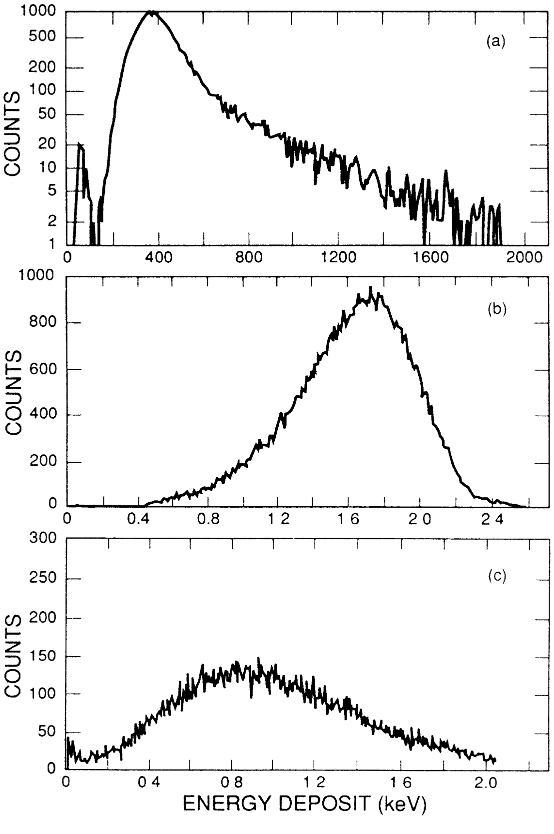

FIG. 8. Detector energy spectra. (a) Backing scintillator. (b) Coincidence counter. (c) Drift chamber.

TABLE II. Summary of electromagnetic corrections.

Spectrum	Coulomb (%/MeV)	Radiative (%/MeV)
^{12}B	−0.09	−0.5
^{12}N	0.05	−0.5

A ray tracing program was written to calculate beta trajectories through the measured fields and investigate the following.

Linearity of momentum versus detected beta position at a fixed field. Beta trajectories were calculated at fields of 2.3, 4.8, and 5.8 kG for beta momenta varying between 50 and 100% of the maximum momentum accepted for each field. For each trajectory the distance d (the distance between the magnet entrance aperture and point of beta detection) was calculated. The relation between beta momentum and d was then fit to a function of the form $p=B\,(kd+b)$ where p is the momentum, B is the magnetic field and k and b are constants. For each field the deviation of the points from the fitted line was $\leq 0.1\%$ (the linearity with which the field was measured). This uncertainty in linearity corresponds to an uncertainty in spectral shape of ~0.05%/MeV at $B=4.8$ and 5.8 kG and 0.01%/MeV for the difference in spectral shape measured at these two fields.

Effect of fringe field saturation. The saturating fringe field serves to decrease the constant k slightly as the magnetic field is increased. A change of 0.4±0.06% in the constant k was found between the fields of 5.8 and 2.3 kG

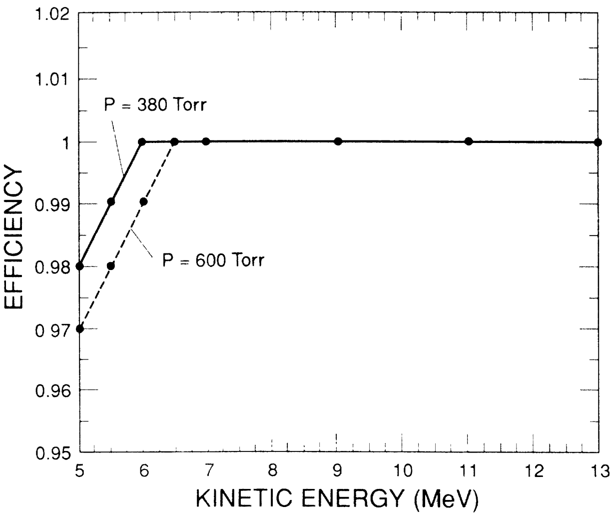

FIG. 9. Calculated spectrograph efficiency. P is the coincidence counter pressure.

TABLE III. Shape factor comparison with theory.

Spectrum	Quantity measured	Theory[a] (%/MeV)	Data (%/MeV)	Total[b] error	Statistical[c] error
^{12}B	α_-	0.41	0.43	0.59	0.53
^{12}N	α_+	−0.52	−0.81	0.69	0.55
^{12}B,^{12}N	$\alpha_- - \alpha_+$	0.93	1.24	0.42	0.33

[a] The uncertainty in these values are ~3% (Ref. 7).

[b] Sum of the statistical error and the systematic errors in Table I.

[c] Quadratic sum of the errors from calibration and the least-square fits to the shape factors.

and a change of 0.15±0.02% was found between the fields of 5.8 and 4.8 kG. These values were used to extrapolate the constant k, measured at 1.5 and 2.14 kG with the ^{40}Ca conversion line, to the higher fields used in the measurements of ^{12}B and ^{12}N. The errors correspond to uncertainties in spectral shape of ~0.01%/MeV for $B = 5.8$ and 4.8 kG.

We conclude that the effect of the magnetic field on the beta spectral shape is understood to within a systematic error of 0.06%/MeV for ^{12}N and ^{12}B and 0.01%/MeV for the ^{12}B − ^{12}N difference.

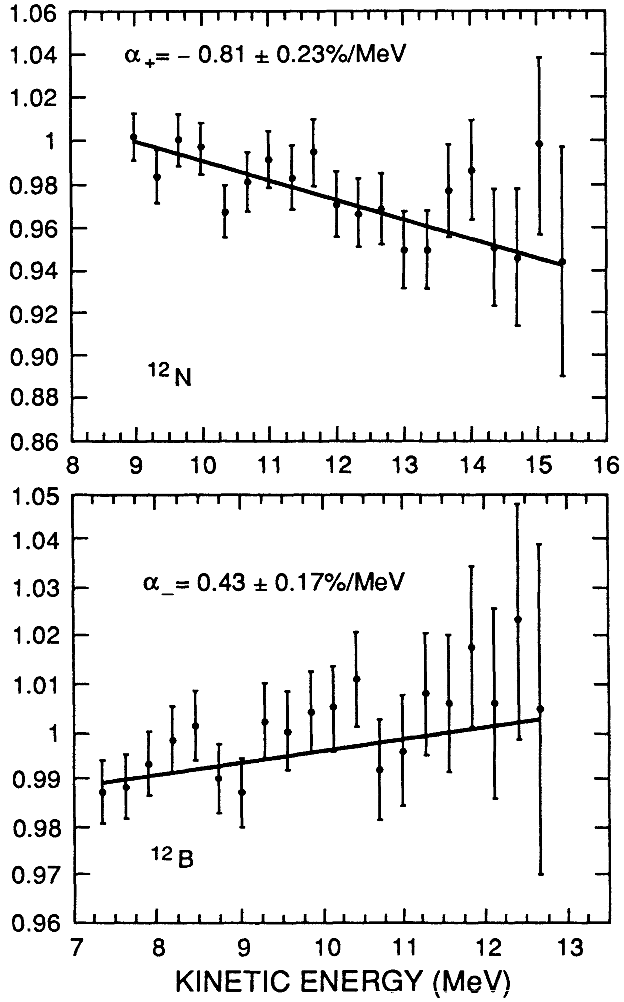

FIG. 10. Corrected shape factors of the ^{12}B and ^{12}N beta decays.

Detector Efficiencies. Figure 8 shows energy spectra for the backing scintillator, coincidence counter, and drift chamber. For both the scintillator and the coincidence counter the fraction of events depositing energy below the respective discriminator levels of 120 and 0.45 keV is less than 0.01%. Figure 8(c) shows energy spectrum $E3$, the energy deposit in wire three from a beta traversing the drift chamber. Discriminator cuts are made at energy deposits of 0.3 and 2.0 keV, resulting in 90% detection efficiency. By using the spectrum PA (already discussed) to correlate beta positions from wires one and three, information from wire one was used to replace the 10% inefficiency in wire three, giving a total drift chamber efficiency of 99%. Software analysis showed no momentum dependence in this final efficiency.

Beta Scattering and Spectrograph Efficiency and Response Function. Energy dependent beta scattering through the targets and detectors was calculated with Cyltran (a Monte Carlo code that models the passage of fast electrons through matter and allows for the simulation of specific geometries).[10,11] For the target thicknesses used (1 and 6 mg/cm^2), the scattering has a negligible effect on the spectra; the small opening angle of the slit (which requires near-normal beta trajectories) minimizes the acceptance of scattered electrons and also restricts the betas to a near-normal path through the target, minimizing scattering. Beta multiple scattering through the coincidence counter and detection system was also modeled with Cyltran. As the beta energy is lowered the scattering in the drift chamber increases until betas are scattered past the scintillator boundary and efficiency is lost. Figure 9 shows the calculated spectrograph efficiency as a function of beta energy. The efficiency is plotted for coincidence counter pressures of 380 and 600 Torr (data were taken at 380 Torr). A deviation from unit efficiency occurs at energies <6.5 MeV,

TABLE IV. Comparison of results with previous work.

Author	$\alpha_- - \alpha_+$
Wu *et al.* (Ref. 8)	0.86±0.24
Kaina *et al.* (Ref. 9)	1.09±0.09
This work	1.24±0.42

well below the lowest energy measured in this experiment.

The total system response function was then calculated. The dominant contributions to its width were source-slit geometry (2%), detector multiple scattering and drift chamber preamp noise (2%). At energies >7 MeV multiple scattering becomes small and the response function is well described by a Gaussian of FWHM ~3%. (An asymmetry in the response function, characteristic of flat-field geometry, arises from the angular divergence of the betas entering the magnet.[12] However the slit restricts the maximum takeoff angle to only 1.5° leaving the asymmetry negligible.) Deconvolution of the response function from the measured beta spectrum had the small spectral effect of ~0.01%/MeV.

Positron In Flight Annihilation. Positrons may annihilate in flight before depositing sufficient energy in the detection system to pass the detection threshold. As this effect varies with positron energy an energy dependent detection efficiency can arise. Deutsch *et al.*[13] have calculated the magnitude of this effect as a function of the threshold energy level. The energy loss required in the thin scintillator is only 120 keV; this produces a slope in the detector efficiency of <0.01%/MeV, a negligible effect. (The energy loss suffered by the betas traversing the gas counters and targets is ~35 keV.) Table I summarizes the effect of the preceding errors on the measured beta spectra.

RESULTS AND CONCLUSIONS

The extraction of $\alpha_\pm$ from the shape factor involves accounting for the electromagnetic corrections to the spectra. We have used the Behrens-Janecke (BJ) function F_{BJ} for the Coulomb correction. For the radiative correction, we use the expression given by Sirlin.[14] The corrections are summarized in Table II.

After subtracting these corrections we present in Fig. 10 the corrected shape factors, the slope of which gives $\alpha_\pm$. In Table III we present values for $\alpha_\pm$ and their comparison with theory.

The errors in the determination of the *individual* shape factors include large statistical contributions from the calibration so that no meaningful conclusion can be drawn from them with regard to CVC. The measurement of the *difference* of the ^{12}B and ^{12}N shape factors constitutes our best experimental test of the CVC theory. This quantity is insensitive to both systematic and calibration errors. We find the quantity $(\alpha_- - \alpha_+)$ in good agreement with theory.

Table IV compares the results of this work with other recent measurements. We conclude that the results of this experiment, while limited by statistics, support the prediction of CVC to the 30% level.

ACKNOWLEDGMENTS

I wish to thank Dr. Gerald Garvey for his help in the design and execution of this experiment. Dr. David Wark is thanked for his help in the early stages of this experiment. The assistance of Dr. Thomas Bowles and Dr. Hamish Robertson in the final data taking run is acknowledged. The Argonne Dynamitron and Los Alamos Tandem staffs are acknowledged for their competent support in this investigation. This work was performed under the auspices of the U.S. Department of Energy by the Los Alamos National Laboratory under Contract No. W-7405-ENG-36.

---

[*] Present address: Physics Division, Los Alamos National Laboratory, Los Alamos, New Mexico 87545.

[1] R. P. Feymann and M. Gell-Mann, Phys. Rev. **109**, 193 (1958).

[2] L. Grenacs, Annu. Rev. Nucl. Part. Sci. **35**, 455 (1987).

[3] M. Gell-mann, Phys. Rev. **111**, 362 (1958).

[4] T. Mayer-Kuckuk and F. Michel, Phys. Rev. **127**, 545 (1962).

[5] N. Glass and R. Peterson, Phys. Rev. **130**, 299 (1962).

[6] Y. K. Lee, L. W. Mo, and C. S. Wu, Phys. Rev. Lett. **10**, 253 (1963).

[7] F. P. Calaprice and B. R. Holstein, Nucl. Phys. **A273**, 301 (1976).

[8] C. S. Wu, Y. K. Lee, and L. W. Mo, Phys. Rev. Lett. **39**, 72 (1977).

[9] W. Kaina, V. Soergel, H. Thies, and N. Trost, Phys. Lett. **70B**, 411 (1977).

[10] J. A. Halbleib and T. A. Melhorm, Sandia National Laboratory Report No. SAND 84-0573, 1984.

[11] M. J. Berger, in *Methods in Computational Physics,* edited by B. Alder (Academic, New York, 1963), Vol. 1.

[12] M. Mladjenovic, in *Development of Magnetic β-Ray Spectroscopy,* edited by W. Beiglbock (Springer-Verlag, New York, 1976), pp. 83–95.

[13] J. P. Deutsch, P. C. Macq, and L. van Elmbt, Phys. Rev. C **15**, 1587 (1977).

[14] A. Sirlin, Phys. Rev. **164**, 1767 (1967).